APPLIED SCIENCES AND ENGINEERING

Neonatal wearable device for colorimetry-based real-time detection of jaundice with simultaneous sensing of vitals

Go Inamori[1], Umihiro Kamoto[1], Fumika Nakamura[1], Yutaka Isoda[2], Azusa Uozumi[3], Ryosuke Matsuda[1], Masaki Shimamura[1], Yusuke Okubo[4], Shuichi Ito[3], Hiroki Ota[1,2]*

Neonatal jaundice occurs in >80% of newborns in the first week of life owing to physiological hyperbilirubinemia. Severe hyperbilirubinemia could cause brain damage owing to its neurotoxicity, a state commonly known as kernicterus. Therefore, periodic bilirubin monitoring is essential to identify infants at-risk and to initiate treatment including phototherapy. However, devices for continuous measurements of bilirubin have not been developed yet. Here, we established a wearable transcutaneous bilirubinometer that also has oxygen saturation (SpO_2) and heart rate (HR) sensing functionalities. Clinical experiments with neonates demonstrated the possibility of simultaneous detection of bilirubin, SpO_2, and HR. Moreover, our device could consistently measure bilirubin during phototherapy. These results demonstrate the potential for development of a combined treatment approach with an automatic link via the wearable bilirubinometer and phototherapy device for optimization of the treatment of neonatal jaundice.

INTRODUCTION

Neonatal jaundice is a physiological phenomenon that occurs in >80% of neonates (*1*) and is usually associated with a good prognosis. However, in severe cases, it can cause permanent neurological damage. Jaundice is caused by high blood levels of bilirubin that deposit in the skin. Eventually, the skin color turns yellowish. Increased amounts of hemoglobin in a prenatal fetus are physiological. Accordingly, hemoglobin is rapidly broken down into bilirubin after birth. The metabolic capacity of the liver in a neonate is immature and is less able to process large amounts of bilirubin. This leads to hyperbilirubinemia. As bilirubin is neurotoxic to the early neonatal brain, the serum level of bilirubin should be consistently and strictly monitored with reference to standard bilirubin levels recorded (i) days after birth and (ii) newborn's weight after birth (*2*–*4*). Abnormal hyperbilirubinemia would cause deposition of bilirubin in the basal ganglia, thus resulting in kernicterus or bilirubin-induced neurologic dysfunction (BIND). Kernicterus causes mental retardation, athetotic cerebral palsy, sensorineural deafness, and upper gaze paralysis. Therefore, newborns who exceed the upper reference limit of bilirubin receive treatment for jaundice, including phototherapy (*2*–*4*). During phototherapy, the entire neonate's body or back is irradiated with blue light. Blue light transforms bilirubin into a hydrosoluble photoisomer that can be easily excreted from the liver into bile and urine (*5*–*7*).

Owing to bilirubin monitoring and phototherapy, kernicterus has been notably decreased in many countries (*8*, *9*). Meanwhile, many neonates born in developing countries are still affected by kernicterus owing to the lack of access to medical equipment. In 2010, it was estimated that 114,000 children died and 75,000 children were left with brain damage as a result of neonatal jaundice (*10*). Neonatal jaundice is one of the leading causes of neonatal death and neonatal brain damage in low- and middle-income countries (*11*, *12*). Even in developed countries, there is a risk of kernicterus, especially in preterm infants (*4*).

In terms of phototherapy, increased risk of mortality in extremely low–birth weight neonates owing to excessive therapy has been reported (*13*). Conversely, the bilirubin levels once reduced by phototherapy rebounded and increased in 4.6% of 7048 neonates (*14*). Furthermore, several short- or long-term adverse effects, such as the interference with maternal-infant bonding, dehydration during treatment, bronze baby syndrome, increased incidence of allergic diseases, and increased incidence of melanoma, have also been reported (*15*). Therefore, both excessive and insufficient phototherapy should be avoided, but it is often difficult to monitor precise bilirubin levels during phototherapy. Continuous measurements of bilirubin levels may contribute to the improvement of quality of phototherapy and patient outcome.

In clinical practice, two bilirubin measurement methods are commonly used: a blood test and optical transcutaneous bilirubinometers. The total serum bilirubin (TSB) is measured most accurately by blood tests, but the test is invasive. As the transcutaneous bilirubinometers are noninvasive and can be easily operated, they are commonly used for initial screenings. The bilirubin level measured by a transcutaneous bilirubinometer is called transcutaneous bilirubin (TcB). Although some differences between TcB and TSB values have been reported (*16*–*20*), TcB is almost matched to TSB. The principle of the transcutaneous bilirubinometer is based on the measurement of absorbance differences through the skin in the spectral regions that correspond to the blue and green colors. Current transcutaneous bilirubinometers with xenon lamps or light-emitting diodes (LEDs), such as Bilichek by Royal Philips, the JM series by Konica Minolta Inc., and Bilicare by Mennen Medical Ltd., are shaped as handheld and associated with high cost (approximately

[1]Department of Mechanical Engineering, Yokohama National University, 79-5 Tokiwadai, Hodogaya-ku, Yokohama, Kanagawa 240-8501, Japan. [2]Graduate School of System Integration, Yokohama National University, 79-5 Tokiwadai, Hodogaya-ku, Yokohama, Kanagawa 240-8501, Japan. [3]Department of Pediatrics, Graduate School of Medicine, Yokohama City University, 3-9 Fukura, Kanazawa-ku, Yokohama, Kanagawa 236-0004, Japan. [4]Division of Cellular and Molecular Toxicology, Biological Safety and Research Center, National Institute of Health Sciences, Tonomachi 3-25-26, Kawasaki, Kanagawa 210-9501, Japan.
*Corresponding author. Email: ota-hiroki-xm@ynu.ac.jp

$5000 to $10,000 per unit) and are too heavy (approximately 200 g) for wearable electronics. Recently, colorimetric methods based on acquired images with a smartphone camera have been researched for bilirubin concentration measurements (*21*, *22*). Colorimetric methods are convenient and noninvasive, but there are difficulties in terms of accuracy. Moreover, it is difficult to make correct bilirubin measurements during phototherapy with handheld bilirubinometers and smartphone methods.

Various wearable devices with organic materials have been extensively developed owing to advances in material technology (*23*–*29*). In particular, wearable devices that can detect multiple vital signs in neonates, such as SpO_2, electroencephalograms, and respiration rates (*30*–*32*), have been developed in recent years. The devices were composed of a hybrid of organic and inorganic materials that achieved soft contact high adhesion between the device and human skin and lightweight characteristics. Currently, wearable devices that can measure bilirubin and vital signs from the forehead have neither been developed nor been demonstrated in neonates. Clinically, the bilirubin concentration is measured on the forehead with a handheld transcutaneous bilirubinometer as mentioned previously. Compared with the chest, back, hands, and feet, the forehead has two advantages: First, it is relatively stable (*33*, *34*), and neonates do not move their heads a lot, and second, because it can be worn without undressing the neonates. From a physiological standpoint, it is better to avoid disturbing neonates to maintain their sleep patterns and calmness.

In this study, we developed a wearable, lightweight, and low-cost bilirubinometer that can noninvasively measure bilirubin levels from the forehead of neonates and also evaluated its functionality in neonates. In addition, we added the ability to measure heart rate (HR) and oxygen saturation (SpO_2) simultaneously to justify its potential for multivital sensing. HR and SpO_2 are common vital signs that are frequently measured in medical procedures. The device previously proposed (*35*) was based on two LEDs and achieved preliminary bilirubin measurement results based on a small number of objectives considered in clinical trials. In the present study, however, we have established the concept of bilirubin measurement through experiments on 50 neonates and neonates treated via phototherapy. Moreover, to obtain high-intensity LED signals for improving the bilirubin measurement accuracy and to realize additional detection of vitals, HR signals and SpO_2, a polydimethylsiloxane (PDMS) lens, and a silicone interface composed of a mixture of blacked PDMS and Ecoflex were developed. The PDMS lens enabled high-intensity signals to be obtained, whereas the silicone interface helped improve the adhesion between the device and skin. In addition, the processing circuit was improved and adjusted to enable acquisition of even smaller signals of reflected light. Consequently, the device provides the possibility to evaluate the conditions of neonatal jaundice, HR, and SpO_2 simultaneously. In this study, our aim was to demonstrate the proof of concept and the potential of our device to change the therapeutic management of neonatal jaundice.

RESULTS

Device design

Figure 1 shows a conceptual schematic of the developed device. The bilirubin levels are measured by the difference of the absorbances of the blue (λ = 460 nm) and green (λ = 570 nm) lights generated with small LEDs (Fig. 1, A and B). The SpO_2 and HR are calculated on the basis of the absorbances of red (λ = 640 nm) and infrared (IR; λ = 950 nm) LED lights. The assembly of these four LEDs in the device provides the capability for the measurements of bilirubin, SpO_2, and HR in neonates. To obtain large intensity signals (reflected lights) of LEDs, a PDMS lens was used in this study to promote the light intensity and silicone interface to improve the adhesion between the device and human skin. In addition, the processing system and display were set up on a smartphone or a personal computer (PC) (Fig. 1B). Figure 2 (A and B) shows the structure and actual

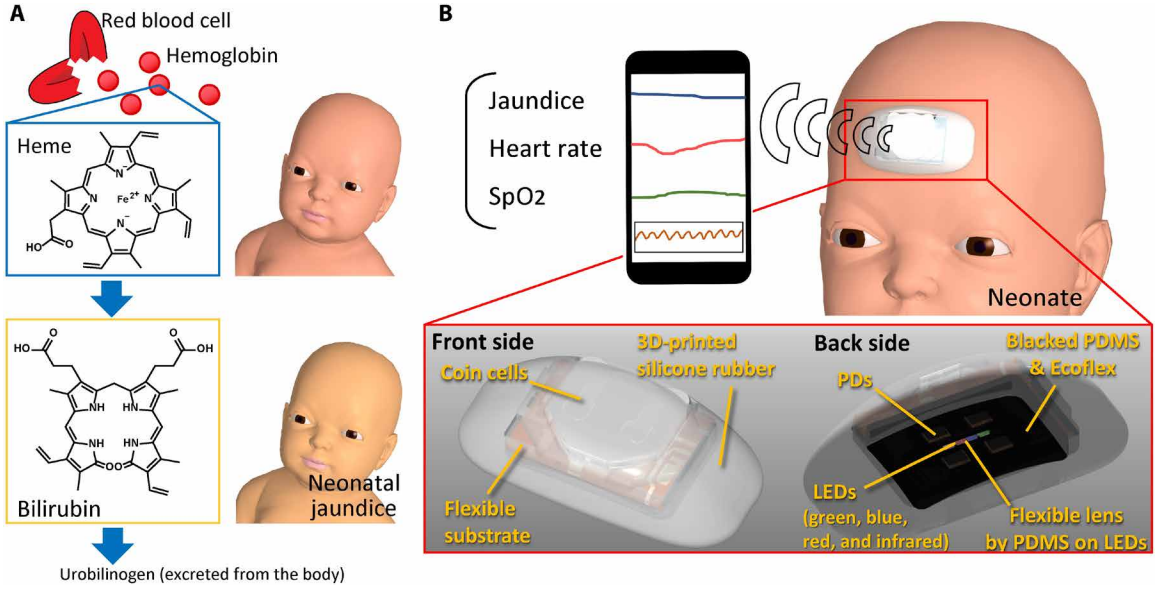

Fig. 1. Conceptual schematic of wearable bilirubinometer. (**A**) Neonatal jaundice is caused by bilirubin that is generated by the breakdown of hemoglobin in red blood cells. (**B**) The stand-alone bilirubinometer is placed on a neonate's forehead. The device is packaged in soft silicone rubber. The bilirubin levels of neonates are measured on the basis of the ratio of absorbances of blue and green lights. The SpO_2 and HR are measured using standard pulse oximeter techniques. The data are transferred to a smartphone or a PC via a Bluetooth connection.

device photographs. The weight of the developed device was 16 g including the coin cells. A circuit on flexible substrates was folded inside the device. The flexible substrate was fabricated by photolithography (fig. S1). The flexible board contains integrated circuits, a Bluetooth low-energy (BLE) module, LEDs, and photodiodes (PDs). The area around the LEDs and PDs was surrounded by black PDMS and Ecoflex mixtures to prevent the lights of the LEDs from wrapping around the PDs directly. A transparent PDMS lens was formed above the LEDs. This made it possible to (i) deliver light to the inner parts of the skin efficiently and (ii) increase the signals of the lights from the LEDs. Blue and green lights were used to measure bilirubin concentrations, and red and IR lights were used to measure the HR and SpO_2 (Fig. 2C). The bilirubin in the skin absorbs blue light. Conversely, other absorbent substances in the skin, including melanin and hemoglobin, absorb green light. The bilirubin concentration was calculated from the ratio of the absorptions of blue and green lights. Although the amount of melanin varies in human species, it has been confirmed that bilirubin could be measured precisely by a transcutaneous jaundice meter regardless of race (*16*). The developed device was attached on the foreheads of neonates (Fig. 2D). Figure 3A and fig. S2 (A and B) show the internal system of the device. The microcontrol unit (MCU) controls the timing of the four-color LED emissions. Figure 3B shows the driving voltage of the LED and the signals detected by the PDs. The temporal span of the cycle was 60 ms, and the lights of green, blue, red, and IR LEDs were emitted once for 4 ms (fig. S2C). PDs detected the light that was reflected through the skin and vessels. Because the PD signal was a weak current signal, an amplifier was used to convert it to a voltage signal and amplify it. In addition, the PDMS lens improved the light intensity received by the PDs (fig. S3). The amplified signal was converted to a digital signal by the analog-to-digital converter (ADC). In terms of the pulse wave, a high-resolution ΔΣADC was used (fig. S4) to calculate SpO_2 from the pulse wave. The measured data were sent to a smartphone via Bluetooth. On the basis of these data, the bilirubin concentration, HR, and SpO_2 were calculated. To elucidate the manner in which light passes through the skin, simulations were performed using a ray-tracing simulation software (figs. S5, A to C, and S6). The simulation showed that the PDMS lens increased the amount of PD light received (fig. S5D). Simulations were also performed to elucidate the relationship among the LED-PD distance (fig. S6A), depth of the optical path, and amount of light received at the PD (fig. S6, B to G).

HR and SpO_2 measurements

The experimental results of SpO_2 and HR are shown in Fig. 4. Figure 4A shows the pulse wave signals. In terms of SpO_2, the calculations were based on Lambert-Beer's law from the reflected red and IR light intensities (*36*). The direct current (DC) value in the SpO_2 measurement was the intensity of the detected light. The alternative current (AC) value was the amplitude of signals from the pulse wave. The ratio of light intensities of red and IR lights (R) was calculated from the AC and DC values in the red and IR LEDs as follows

$$R = \frac{AC_{Red}/DC_{Red}}{AC_{IR}/DC_{IR}} \quad (1)$$

SpO_2 was derived from the following equation

$$SpO_2 = \frac{\varepsilon_{Hb}(\lambda_{Red}) - \varepsilon_{Hb}(\lambda_{IR}) \cdot R}{(\varepsilon_{Hb}(\lambda_{Red}) - \varepsilon_{HbO_2}(\lambda_{Red})) + (\varepsilon_{HbO_2}(\lambda_{IR}) - \varepsilon_{Hb}(\lambda_{IR})) \cdot R} \times 100 + A \quad (2)$$

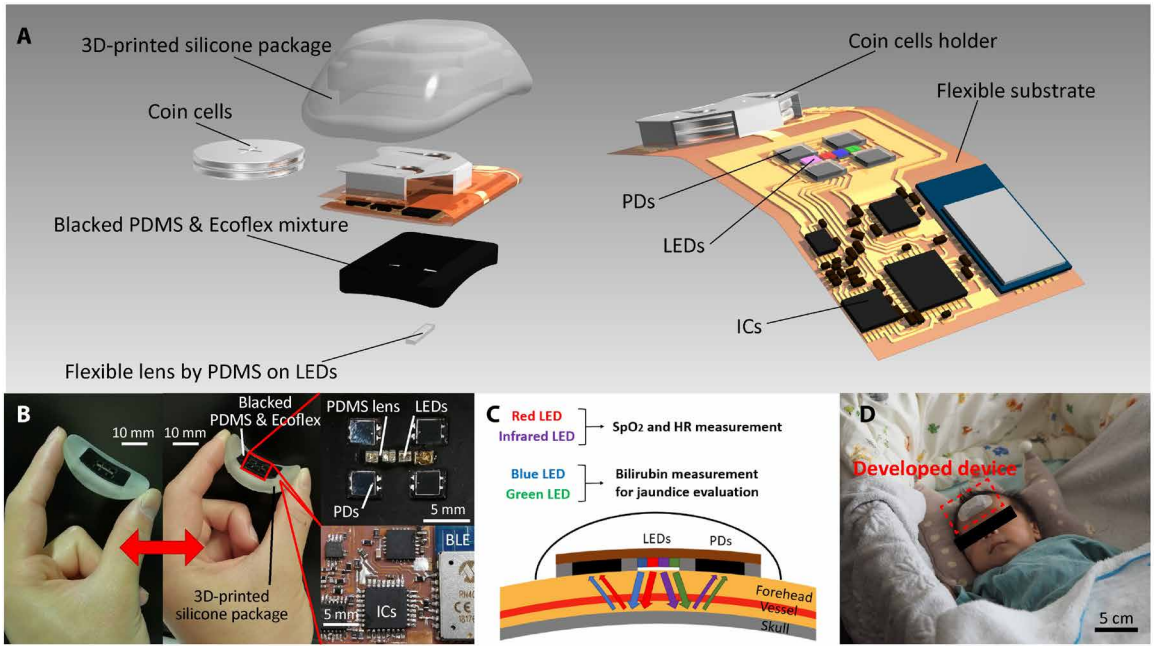

Fig. 2. Structure of the actual wearable bilirubinometer. (**A**) All electronic components are mounted on a flexible substrate. Coin cells are used to serve as the battery. LEDs and PDs are surrounded by a blacked PDMS and Ecoflex mixture. The flexible PDMS lens is formed on the LEDs. The package is made of three-dimensionally (3D) printed flexible silicone. ICs, integrated circuits. (**B**) Photograph of the actual device, sensing part that contacts neonate's forehead, and a circuit that conducts the control and processing tasks. Photo credit: Go Inamori, Yokohama National University. (**C**) Cross-sectional schematics of sensing mechanism and contact of the device. (**D**) Photograph of the device on a neonate. Photo credit: Ota Hiroki, Yokohama National University.

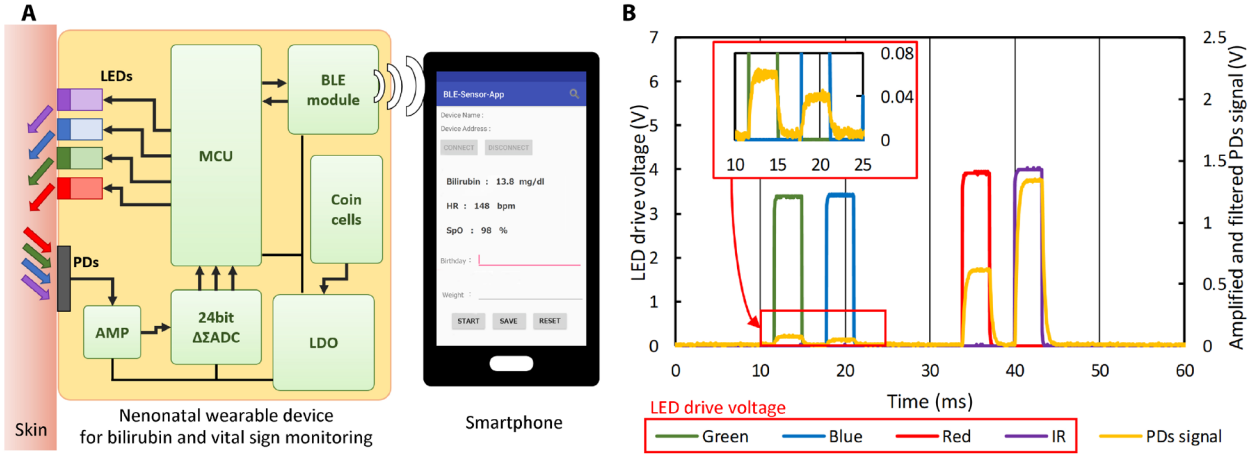

Fig. 3. System diagram of the device. (**A**) Block diagram of the device. The LEDs are controlled by the MCU. Signals are amplified by the amplifier and converted to a digital form by the ADC. The data are transferred to a smartphone. The low-dropout (LDO) stabilizes the voltage of the coin cells. (**B**) Green, blue, red, and IR LEDs emit for 4 ms. The switching of the emission is controlled by MCU. Signals are detected by the PDs and analyzed to measure SpO_2, HR, and bilirubin.

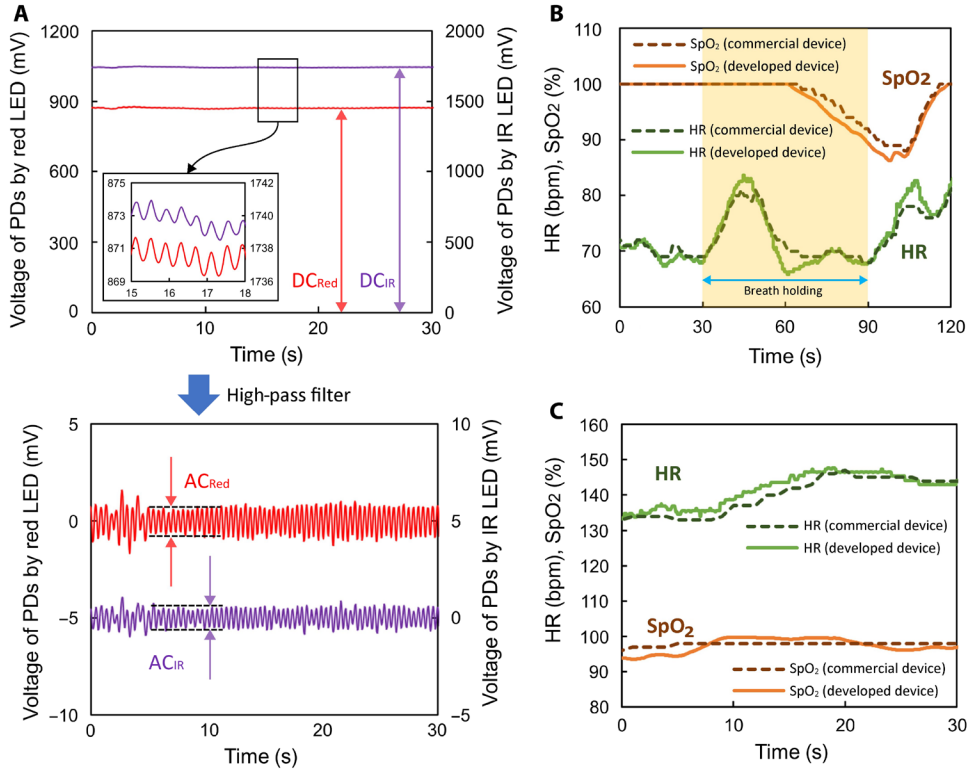

Fig. 4. HR and SpO_2 measurements. (**A**) Variations of voltage values detected in PDs by the reflected red and IR lights. Pulse wave was observed by the red and IR lights. (**B**) Measurements of HR and SpO_2 conducted by the developed and commercial devices before, during, and after holding the breath for 1 min in adults. SpO_2 decreased considerably 60 s after the onset of breathholding. (**C**) HR and SpO_2 measurements in a neonate.

where ε_{Hb} and ε_{HbO_2} are the absorption coefficients of deoxyhemoglobin (Hb) and oxyhemoglobin (HbO_2) at wavelength λ (red and IR lights), and A is the calibration constant. The HR was calculated as the number of beats per minute from the wave period of the reflected light.

As shown in Fig. 4B, the measurement of SpO_2 by the developed device and a commercial device was conducted before, during, and after holding the breath. The device and a commercial pulse oximeter were worn on the forehead of an adult simultaneously. The SpO_2 started to decrease 30 s after the onset of the breathhold and significantly dropped for 30 s. After breathing resumed, it returned to normal levels in 25 s. The values of HR and SpO_2 in a neonate measured by the developed device matched the values of the commercial device (Fig. 4C). Movie S1 shows actual detections of bilirubin, SpO_2, and HR using the developed device on an adult forehead. In the commercial device, the processing diagram of the signals of HR or SpO_2 is unknown and may be different from the developed device. This explains why there is a minor difference between the results.

Bilirubin concentration measurement for the evaluation of neonatal jaundice

The principle of bilirubin concentration measurement is based on the comparison between the light intensities of reflected blue and green LEDs based on Lambert-Beer's law. Before the clinical experiments, the light absorption of bilirubin in the blue and green spectral regions was confirmed in vitro. As shown in fig. S7A, blue and green LEDs were irradiated from the top. The PD under the chamber that contained the bilirubin solution detected the blue and green light intensities through the solution. Figure S7B shows the relationship between the light intensities of the blue and green LEDs though the bilirubin solution and the concentration of bilirubin in the solution. It was confirmed that the light that passed through the solution decreased with respect to the bilirubin concentration. In addition, the light intensity of the blue LED diminished more than that of green light. The decrease in the signals followed the theoretical value derived from Lambert-Beer's law. On the basis of Lambert-Beer's law, the following formula was used to calculate bilirubin concentration in neonates (see the Supplementary Materials)

$$C = D \cdot \log_{10}\left(E \cdot \frac{I_{\mathrm{Green}}{}^{\alpha}}{I_{\mathrm{Blue}}}\right) \quad (3)$$

where C is the bilirubin concentration, I_{Green} and I_{Blue} are the reflected light intensities of the green and blue lights, D is the calibration constant for the optical path length, E is the calibration constant for LED emission, and α is the calibration constant for the weighting of the blue and green lights. Three constants, D, E, and α, were derived from the minimum values of the mean difference (MD), doubled SD (2SD) in the Bland-Altman method (*37*), and the maximum value of correlation coefficient R in the relationship between the values of the developed device and commercial handheld bilirubinometer.

The results of the experiments with normal neonates are shown in Fig. 5 (A and B). In these experiments, we measured 50 neonates 1 to 7 days after birth. The calibration constants were determined by comparing the measurements of the developed device with those of the commercial, handheld bilirubinometer. The correlation of the results obtained by the commercial handheld bilirubinometer and the developed devices was confirmed, as shown in Fig. 5A. The correlation coefficient was $R = 0.81$. The SD of the difference was 2SD = 4.6 (Fig. 5B). The average value of the errors was zero because the calibration constant was determined to be zero in the case of the MD. In addition, TcB was measured using the developed device and commercial bilirubinometer six times during 6 hours (fig. S8), because bilirubin in a neonate increases on an hour scale not on second and minute scales. During these 6 hours, the TcB of a neonate 3 days after birth was confirmed to increase based on the results obtained using a commercial bilirubinometer. Although the deviation of the developed device was larger than that of the commercial bilirubinometer, the results obtained using the developed device also exhibited an increasing trend. The results from the simultaneous measurements of bilirubin concentration, HR, and SpO_2 are shown in Fig. 5C. The device was attached to the forehead of a neonate, and the measurement process was performed. As the commercial handheld bilirubinometer could not be used simultaneously with the developed device, the measurements obtained by using the former device were recorded immediately before this measurement process. The bilirubin concentration as measured by the developed device was displayed every 20 s based on the blue and green reflected light values acquired during the previous 20-s interval. This experiment demonstrated that the bilirubin concentration, HR, and SpO_2 can be measured simultaneously.

Clinical phototherapy experiments

Clinical experiments were conducted on neonates who underwent phototherapy. TcB measured by the developed device and TSB were compared before, during, and after phototherapy. During phototherapy, the light was generated from the anterior or posterior side of the neonates according to the patient's severity level (Fig. 5D). In severe cases of neonatal jaundice, the neonate was exposed to blue light from the anterior side to irradiate the entire body with the light (Fig. 5E). Conversely, a neonate with mild jaundice was exposed to the light from the posterior side (Fig. 5F). The device was set on the area hidden by the eye mask that protected the neonate's eyes from blue light irradiation during phototherapy. This eye mask prevented the blue light from decomposing the bilirubin directly. A gradual decrease in the bilirubin levels following the initiation of phototherapy was observed in neonates who were exposed to the blue light from either the anterior or posterior direction (Fig. 5, E and F). In both cases, the TcB measured by the developed device was matched to TSB. The error between the two methods was within approximately 3 mg/dl. In the case of phototherapy from the anterior side (Fig. 5E), the measurements obtained using the developed device and TSB were performed 24 hours after the treatment (fig. S9). The results of the device followed the TSB values (fig. S9). The bilirubin levels stabilized after 24 hours, and the device was observed to perform well even 24 hours after the treatment.

DISCUSSION

In this study, we developed a small and lightweight wearable device that can measure bilirubin concentration, HR, and SpO_2 simultaneously. The developed device weighs 16 g including the coin cells. Its weight is less than one 10th that of conventional bilirubinometers. It also showed the possibility of measuring bilirubin concentration during phototherapy. HR and SpO_2 measured by pulse oximeters are two of the most fundamental vital signs in medical practice. Currently, measurements are performed with sensors connected to equipment via cables. Wearable devices for detecting SpO_2 in neonates with flexible and stretchable substrates have also been developed (*30*, *31*). The measurements were conducted on the feet of neonates. In this study, the developed device combined jaundice, SpO_2, and HR sensing from the foreheads of neonates.

We chose the forehead as the measurement site because it has several advantages. First, it is convenient to attach the device on the forehead because the neonates do not need to be undressed. Second, the forehead is one of the most stable sites. Usually, hands and feet are chosen for the measurements of SpO_2 in neonates, but these are often affected by their body motions. As neonates cannot roll over or move their heads violently, the forehead is an ideal site for continuous HR and SpO_2 monitoring (*38*). Third, the optical sensing of the vital signs through the blood vessels is easily achieved on the basis of forehead recordings because the supratrochlear artery is present between the skin and skull on the forehead. The detection of jaundice, HR, and SpO_2 with one device placed on the forehead of neonates could reduce the burden on both the medical staff and the neonate. SpO_2 measurements at the forehead are more responsive to changes than hand measurements (*33*, *39*). This

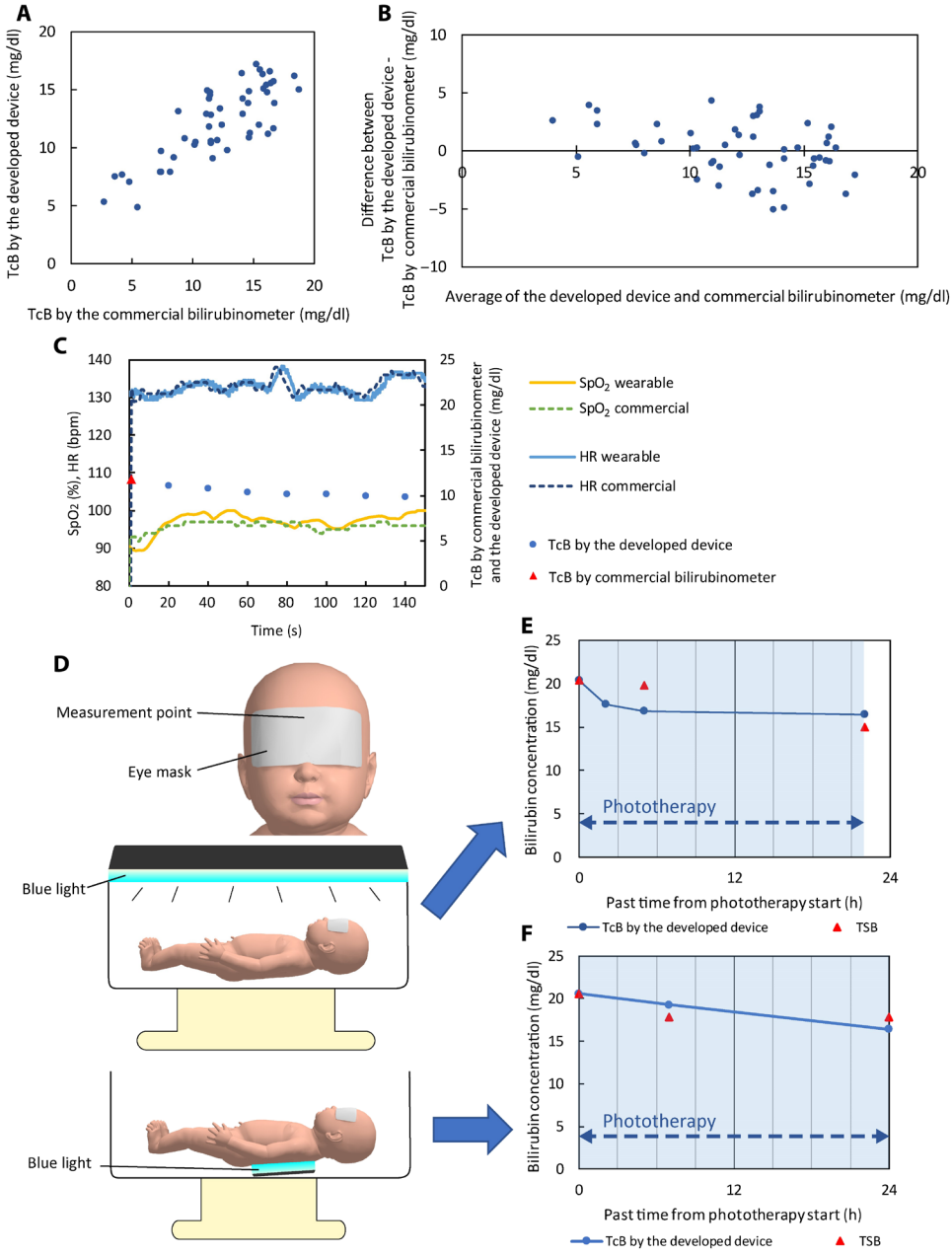

Fig. 5. Bilirubin measurements using the developed device. (**A**) Relationship between the wearable device and the conventional transcutaneous bilirubinometer in 50 neonates. The correlation coefficient of the data obtained by the meters was 0.81. (**B**) A Bland-Altman plot of the wearable device and the commercial transcutaneous bilirubinometer. MD = 0 and 2SD = 4.6. (**C**) Simultaneous measurement of HR, SpO_2, and bilirubin concentration using the developed device. (**D**) Schematic of condition of neonates during phototherapy. Neonates were exposed to blue light for the therapy from the top and bottom according to a patient's severity level. (**E** and **F**) Bilirubin measurements using the developed device and blood test during phototherapy following blue light exposure from the top (anteriorly) (D) and the bottom (posteriorly) (E). TcB by the developed device matched TSB.

may be useful for the early detection of neonatal apnea and other critical conditions.

In this study, the PDMS lens between the LEDs and the skin was formed to deliver light more efficiently to the neonatal skin. The simulation results indicated an increase in the light intensity under the skin surface (fig. S5D). The reflected light signal obtained at the forehead of the neonate was not enough to acquire the precise value of bilirubin in the skins of the neonates. By forming the PDMS lens on top of the LEDs, the PDs obtained signals from the reflected light through the human skin 1.1 to 2.5 times higher than those of the device without the lens (fig. S3, A and B). Two reasons may explain this finding. First, the flexible lens may prevent reflection by the skin surface. Any gap between the skin and the LEDs decreased the light intensities considerably. The flexible lens by the PDMS that contacted the neonate foreheads prevented the reflection and diffusion of the lights on the surface of skin and eventually promoted the reflected light in the skull through the skin. Second, the refraction by the PDMS lens allowed the light to be spread over a wider area.

Figure S3C shows the observation of the LED light parts at an oblique angle with and without PDMS. In the left side of fig. S3C, which shows the LED part without the PDMS lens, the LED light was not visible. Conversely, in the right side of the figure, which shows the LED part with the PDMS lens, LED lights were observed clearly. Because of the refraction through the PDMS lens, the light spreads over a wider area. This leads to an increase in PD signals in all colors. It is important to decrease the energy consumption for long-term use with small coin cells or a battery because it is difficult to use high voltages and large batteries (such as the Li-Po battery) for medical use for the sake of safety. Therefore, the increase in the light intensity signals based on structural optimization is crucial for the wearable device of vital sensing for neonates.

In this study, the *R*, MD, and 2SD values calculated based on data from 50 neonates were 0.81, 0, and 4.6, respectively, compared with TcB measured by the commercial handheld bilirubinometer. Conversely, compared with TSB, the *R*, MD, and 2SD values were 0.72, −0.7, and 5.6 (of 15), respectively, as shown in fig. S10 (A and B). TcB values at high bilirubin densities were lower than that shown in fig. S10. This is consistent with the results of other research studies (*16*, *40*, *41*) conducted using JM-103 (*20*), an older model of the JM-105 used in this study. In fig. S10, TcB values obtained using the JM-105 at high bilirubin densities agreed with the results of TSB measurement. This implies that the detection system of the JM-105 might be better. To improve the accuracy of the developed device over the entire range of results in Fig. 5, correction parameters could be considered for the high-density range based on measurements from more cases. In terms of the commonly used handheld bilirubinometers by Konica Minolta, Philips, and Mennen, the *R*, MD, and 2SD values between TcB by these bilirubinometers and TSB have been reported to be in the ranges of 0.77 to 0.93, −1.6 to 0.5, and 2.76 to 3.8, respectively (*16*–*20*). The *R*, MD, and 2SD outcomes were slightly better than those of our devices. The differences of the results were attributed to the stability of the adhesion and pressure between the device and the skin. The presence of space between the device and skin causes reflection of light from the surface of the forehead skin, which leads to inaccurate results. Similarly, the pressure variation between the device and skin might alter the thickness of the skin, which, in turn, affects *d* (the optical path length) as per eq. S1 and leads to an inaccurate result. In light of the results above, we acknowledge that for commercial adoption, we will need to further improve the stability and accuracy of the device. In terms of the commercial bilirubinometers, the pressures developed when the bilirubinometers contacted the skin of the neonates were controlled by a spring structure. In future work, to improve the sensitivity of the developed device, the adhesive and interface between the device and forehead should be optimized. Simultaneously, a neonate headband can be used to stabilize the position of the device and maintain a constant pressure between the device and forehead.

In this study, experiments were also conducted in neonates undergoing phototherapy. In the cases depicted in Fig. 5 (E and F), TcB obtained by the developed device was well matched to TSB. As shown in fig. S11, no noise was caused by environmental lights or the blue light from phototherapy devices. This is because the interface composed of a black-colored mixture of PDMS and Ecoflex covered the forehead and prevented light from the environment and the phototherapy device from entering the space between the device and the forehead. In terms of commercial bilirubinometers, for precise measurement, a light-shielding patch must be attached to the measurement area of the neonatal forehead and removed for each measurement during phototherapy (*42*). Conversely, our device itself may be able to block the blue light and measure the bilirubin level even during phototherapy given that it can be placed on the forehead as a wearable device. Continuous monitoring of bilirubin may avoid excessive or insufficient phototherapy treatments and can thus result in the reduction of side effects of overexposure to blue light and the reduction of workload for the medical staff.

Recently, new methods have been developed to estimate the bilirubin concentration based on the capture of skin color images using smartphones. This method is quite convenient and low cost. Actually, only a smartphone with a camera and a dedicated app were required. However, the accuracy of this method has been reported to vary widely, with R = 0.48 to 0.91 (*21*, *22*, *43*, *44*). The measurements were affected by the surrounding environment. During phototherapy, a light-shielding patch must be attached to the measurement area even with the method that uses a smartphone camera, just like a conventional bilirubinometer. Conversely, using our device, measurements can be conducted during phototherapy if the device is worn throughout the therapy given that the device itself blocks light. In addition, our device has the potential to measure SpO_2 and HR at the same time.

We achieved a large decrease in the device weight to allow its potential use as a wearable device. The final weight was 16 g, which is less than $^1/_{10}$ of the 200 g of a conventional bilirubinometer (JM-105, Konica Minolta). By contrast, the weight of eye mask during phototherapy is approximately 1 to 2 g. Ideally, the weight of our device should be reduced by an additional $^1/_{10}$ of the current weight. Organic LEDs (OLEDs), organic PDs (OPDs), and flexible batteries would help decrease the weight even further. As shown in table S1, the weight of the three-dimensionally (3D) printed silicone package, blacked PDMS and Ecoflex mixture, coin cells, and coin cell holder constitutes the majority of the weight of the device. By using an OLED and OPD, the volume of the 3D-printed silicone package and blacked PDMS and Ecoflex mixture, whose weight constitutes half of the total weight of the device, can be effectively reduced. Similarly, using a flexible battery would decrease the weight of the batteries and the package as well as eliminate the need for a battery holder. In addition, the materials used for skin-device interface need to be modified for long-term use, especially given the thin and fragile skin of a neonate. In this regard, the breathability of the material is an important factor (*45*). In addition, we need to use softer and milder materials suitable for the delicate neonatal skin.

In particular, there are two limitations of this study that could be addressed in future research. First, the device's current accuracy is not sufficient to allow for its use in clinical decision making in medical practice. This insufficient accuracy can be addressed via further improvement of the adhesion between the skin and the device and by stabilizing the pressure of the device exerted on the skin. Second, the interface between the package and skin is flexible, but the circuitry and battery are not flexible. However, the flexibility of this part can be improved by using a more flexible substrate, such as a thinner polyimide film or parylene, as well as a flexible battery. More flexible and thinner devices may potentially improve the accuracy by facilitating better contact with the skin.

In future work, the development of a combined treatment device that is automatically linked to the wearable bilirubinometer and a

phototherapy device can optimize the treatment of neonatal jaundice. In addition, by making it possible to apply the technique to home health care, it will be possible to detect jaundice after a patient is discharged from a hospital.

In summary, we have developed a wearable device for neonates that can measure bilirubin levels and vital signs using LEDs. In this device, a flexible lens made of PDMS was assembled on LEDs and PDs to achieve excellent contact between the sensing part and the skin, making the transmission of the lights more efficient. This device has the potential to realize continuous bilirubin concentration monitoring conveniently and at a low cost. Our device may be easily connected with phototherapy equipment that realizes the optimization of the therapeutic strategy and the implementation of semi-automated treatment. This combination therapy may lead to the prevention of side effects of excessive phototherapy and to the reduction of kernicterus or BIND owing to insufficient treatment. In addition, it may also decrease the burden on neonates and medical staff.

MATERIALS AND METHODS

Device fabrication

The structure of the device is shown in Fig. 2A and fig. S1. The circuit of this device was fabricated by photolithography on a flexible substrate made of polyimide. Small electric components, including the MCU (Atmega328p, Microchip Technology), BLE (RN4020, Microchip Technology), low-dropout regulator (LDO; TPS7A47, Texas Instruments), ADC (ADS1220, Texas Instruments), amplifier (NJM2732RB-TE1, New Japan Radio), blue LED (KPTD-1608QBC-D, Kingbright), green LED (KPTD-1608CGCK, Kingbright), red LED (KPTD-1608SEC/J3, Kingbright), IR LED (SFH4441, OSRAM), PDs (VBPW34S, Vishay), resistors, and capacitors, were mounted on the substrate. The flexible lens used for the improvement of the light intensity of the LED was formed by PDMS (SYLGARD 184 Silicone Elastomer, Dow Corning) on the LEDs. This PDMS on the LEDs enables efficient light delivery to the skin (fig. S3). The area meant to be in contact with the neonate's forehead was made of a black-colored mixture of PDMS and Ecoflex (Ecoflex 00-30, Smooth-On) by pouring it into a 3D-printed mold to (i) increase the adhesion between the device and the foreheads of neonates and (ii) prevent the light from illuminating the PDs directly without reflection. The entire device was packaged with 3D-printed silicone rubber manufactured using a 3D printer (Agilista, Keyence).

The head circumference range in neonates is approximately 30 to 38 cm (*46*), and the radius is approximately in the range of 48 to 61 mm. On the basis of this information, we designed the curvature of the device package to be 55 mm. The deformability of the interface formed using the 3D-printed package (fig. S12, A and B) and black-colored PDMS and Ecoflex mixture (fig. S13) can cover the difference between neonates. As shown in fig. S12, the softness of the 3D-printed package is similar to that of PDMS, which is a soft material with sufficient flexibility used for flexible devices (fig. S12C). In addition, the black-colored mixture of PDMS and Ecoflex could cover a head with a radius in the range of 47.5 to 62.5 mm (fig. S13, A and B). This prevents the light of the LEDs from reflecting on the skin or being admitted into PDs directly through the space between skin and device.

All the materials used in the device, including PDMS, Ecoflex, and 3D-printed silicone rubber, are widely used commercial materials having high biocompatibility. In addition, the black ink (Silc Pig, Smooth-On) is approved for use based on the 2012 Occupational Safety and Health Administration Hazard Communication Standard 29 Code of Federal Regulations 1910.1200 criteria and does not contain harmful material.

System diagram

The measurement system is shown in Fig. 3A. The MCU controlled the timing of LED emission (fig. S2C). The driving currents and irradiance values of the LEDs are shown in table S2 and fig. S14 (A and B), respectively. It is difficult for blue and green lights to penetrate through the skin. In addition, the sensitivity of the PDs to blue and green light was low. Therefore, the device could not properly measure bilirubin levels using only one PD. Hence, the amount of reflected light that passed through the neonate's skin was measured via four PDs. Moreover, compared to a single PD, four PDs could capture the reflected lights in all directions more efficiently. The signal was amplified by an amplifier. The noise in the signals was removed by the low-pass filter (fig. S2D). In terms of blue and green lights used for bilirubin measurements, the signals were very weak compared with those of the red and IR lights. For this reason, the blue and green LED signals were amplified again by a programmable gain amplifier. The amplified signals were converted to a digital signal by the ADC (fig. S4). The data were converted to digital form and were sent to the MCU via a serial peripheral interface communication link (fig. S2E). The MCU sent a signal to the BLE module that was transferred to the smartphone via Bluetooth. The data were recorded in the smartphone and calculated.

In the experiments, raw data were transferred to and recorded on a smartphone or PC. The theoretical background related to the calculation is explained in the Supplementary Materials. The value of the theoretical constant was determined by comparing the raw data and the result obtained using the commercial bilirubinometer. The values were calculated for each device. On the basis of the values, the data were calculated in real time. Eventually, the bilirubin amount, HR, and SpO_2 could be displayed in real time on a PC (movie S1).

Power supply

In the developed device, the battery was based on two coin cells (CR2016). This is because coin cells are safer for medical use compared with lithium batteries. However, the voltage drop was significant. Therefore, the voltage in the device was stabilized by using an LDO regulator. As shown in fig. S15, the lifetime of the batteries was 7 hours when the device was used, which measured bilirubin every 20 min, SpO_2 and HR every 60 ms, and BLE connection every 1 s.

In vitro bilirubin concentration measurements

We conducted in vitro experiments of light absorptions of the blue and green lights through bilirubin (fig. S7). As shown in fig. S7A, the bilirubin solution was exposed to blue and green LEDs from the top. The intensity of light that passed through the solution was measured by a PD placed underneath the solution. Aqueous metasilicate solution was used as a solvent because bilirubin is insoluble in water. Bilirubin concentrations were adjusted in the range from 0 to 11 mg/dl (fig. S7B). The LEDs and the PD were aligned by a jig. The experiment was performed in a dark room to exclude any effects owing to environmental lights.

Optical simulation

Ray-tracing simulations were performed (figs. S5 and S6) using ray-tracing simulation software (LightTools 9.0.0, Synopsys Inc.)—a ray-tracing simulation software based on the Monte Carlo method (fig. S5B). The simulation of biological tissue is based on the Henyey-Greenstein scattering (*47*). This software has also been used to simulate biological tissues and pulse oximeters in other studies (*48*–*50*). A model of the device was constructed on the basis of the LED and PD arrangements, and the characteristics of the device are shown in Fig. 2B. In the simulation, we used a skin model consisting of five layers: epidermis, dermis, subcutaneous tissue, frontalis muscle, and the skull. The depth from the skin surface to the skull was set to 2.9 mm (*51*). The thickness of each layer was set such that the thickness ratio of each layer was equal to that of adult tissues (*52*). The optical properties of each tissue were set on the basis of previous reports (*53*–*56*). Two areas of irradiance measurement were set up: the first area was the sensing surface of the PD, simulating the light emitted by the LED, passing through the skin, and reaching the PD; and the second area was a cross section between the LED and PD, set to detect only the light reaching the PD after passing through this cross section, simulating the depth of the optical path along which the light from the LED traveled to reach the PD.

Clinical experiments

The research protocol was approved by the ethics committee of the Yokohama City University Graduate School of Medicine (no. B190200011, approved on 19 March 2019). This study was carried out in accordance with the Declaration of Helsinki and the Japanese Ethical Guidelines of the Ministry of Health, Labor, and Welfare, Japan. Measurements were performed on neonates with a gestational age of at least 36 weeks. After informed consent from at least one parent was obtained (for all participants), the developed devices were placed on the forehead of the studied neonates by a trained research doctor. The measurement data were collected by a smartphone and were then extracted to a PC. To protect the privacy of the participants, personally identifiable information was stored securely in the hospital.

HR and SpO_2 measurement in clinical experiments

The measurements of HR and SpO_2 were also conducted in adults with the developed and commercial devices. A commercial pulse oximeter for neonates (Neo Pulse, ATOM MEDICAL) was used to measure the standard SpO_2 and HR values. To acquire the calibration of SpO_2 and compare the values between the commercial and the developed devices, devices were attached to the adult's forehead. The data were obtained from the 30-s period that preceded breath-holding until the end of the 30-s period after the subsequent onset of breathing. In terms of the SpO_2 measurements in neonates, SpO_2 was acquired from a commercial SpO_2 sensor (OXISENSOR III N-25, Nellcor) from the feet. The measurement of the SpO_2 by the developed device was performed from the foreheads of the tested neonates.

Bilirubin measurements

All clinical measurements of bilirubin concentration were conducted in neonates between 0 and 7 days after birth. To measure TcB in neonates, a noninvasive, commercial handheld bilirubinometer (JM-105, Konica Minolta) was used. The TcB measurements were conducted in 50 neonates. A blood test using a Bili-Meter E (Atom Medical) was performed in 15 neonates. To demonstrate the measurement of bilirubin levels during phototherapy (Neoblue, Atom Medical), the measurements obtained by the developed device and blood tests were simultaneously conducted in neonates who revealed higher bilirubin levels than standard levels.

Measurement of noise from environmental light and phototherapy devices

The noise caused by lights from the environment and phototherapy devices was measured (fig. S11). This measurement was carried out with the device placed on an adult arm in a darkroom instead of on a neonate. The blue light was set 30 cm from the arm, because the light is far from the neonate during actual medical practices. The signal of the PD was measured with the LED emitting light and not emitting light and was consistent irrespective of whether the lights in the environment (room lights) and phototherapy device were turned on.

SUPPLEMENTARY MATERIALS

Supplementary material for this article is available at http://advances.sciencemag.org/cgi/content/full/7/10/eabe3793/DC1

View/request a protocol for this paper from *Bio-protocol*.

REFERENCES AND NOTES

1. V. K. Bhutani, A. R. Stark, L. C. Lazzeroni, R. Poland, G. R. Gourley, S. Kazmierczak, L. Meloy, A. E. Burgos, J. Y. Hall, D. K. Stevenson; Initial Clinical Testing Evaluation and Risk Assessment for Universal Screening for Hyperbilirubinemia Study Group, Predischarge screening for severe neonatal hyperbilirubinemia identifies infants who need phototherapy. *J. Pediatr.* **162**, 477–482.e1 (2013).
2. M. J. Maisels, V. K. Bhutani, D. Bogen, T. B. Newman, A. R. Stark, J. F. Watchko, Hyperbilirubinemia in the newborn infant > or =35 weeks' gestation: An update with clarifications. *Pediatrics* **124**, 1193–1198 (2009).
3. American Academy of Pediatrics Subcommittee on Hyperbilirubinemia, Management of hyperbilirubinemia in the newborn infant 35 or more weeks of gestation. *Pediatrics* **114**, 297–316 (2004).
4. I. Morioka, Hyperbilirubinemia in preterm infants in Japan: New treatment criteria. *Pediatr. Int.* **60**, 684–690 (2018).
5. S. Onishi, K. Isobe, S. Itoh, M. Manabe, K. Sasaki, R. Fukuzaki, T. Yamakawa, Metabolism of bilirubin and its photoisomers in newborn infants during phototherapy. *J. Biochem.* **100**, 789–795 (1986).
6. S. Onishi, I. Miura, K. Isobe, S. Itoh, T. Ogino, T. Yokoyama, T. Yamakawa, Structure and thermal interconversion of cyclobilirubin IX α. *J. Biochem.* **218**, 667–676 (1984).
7. D. A. Lightner, A. F. McDonagh, Molecular mechanisms of phototherapy for neonatal jaundice. *Acc. Chem. Res.* **17**, 417–424 (1984).
8. M. Sgro, S. Kandasamy, V. Shah, M. Ofner, D. Campbell, Severe neonatal hyperbilirubinemia decreased after the 2007 Canadian guidelines. *J. Pediatr.* **171**, 43–47 (2016).
9. M. W. Kuzniewicz, G. J. Escobar, T. B. Newman, Impact of universal bilirubin screening on severe hyperbilirubinemia and phototherapy use. *Pediatrics* **124**, 1031–1039 (2009).
10. V. K. Bhutani, A. Zipursky, H. Blencowe, R. Khanna, M. Sgro, F. Ebbesen, J. Bell, R. Mori, T. M. Slusher, N. Fahmy, V. K. Paul, L. Du, A. A. Okolo, M.-F. de Almeida, B. O. Olusanya, P. Kumar, S. Cousens, J. E. Lawn, Neonatal hyperbilirubinemia and rhesus disease of the newborn: Incidence and impairment estimates for 2010 at Regional and Global levels. *Pediatr. Res.* **74**, 86–100 (2013).
11. C. Greco, G. Arnolda, N.-Y. Boo, I. F. Iskander, A. A. Okolo, R. Rohsiswatmo, S. M. Shapiro, J. Watchko, R. P. Wennberg, C. Tiribelli, C. D. C. Zabetta, Neonatal jaundice in low- and middle-income countries: Lessons and future directions from the 2015 Don Ostrow Trieste yellow retreat. *Neonatology* **110**, 172–180 (2016).
12. T. M. Slusher, T. G. Zamora, D. Appiah, J. U. Stanke, M. A. Strand, B. W. Lee, S. B. Richardson, E. M. Keating, A. M. Siddappa, B. O. Olusanya, Burden of severe neonatal jaundice: A systematic review and meta-analysis. *BMJ Paediatr. Open.* **1**, e000105 (2017).
13. B. H. Morris, W. Oh, J. E. Tyson, D. K. Stevenson, D. L. Phelps, T. M. O'Shea, G. E. McDavid, R. L. Perritt, K. P. Van Meurs, B. R. Vohr, C. Grisby, Q. Yao, C. Pedroza, A. Das, W. K. Poole, W. A. Carlo, S. Duara, A. R. Laptook, W. A. Salhab, S. Shankaran, B. B. Poindexter, A. A. Fanaroff, M. C. Walsh, M. R. Rasmussen, B. J. Stoll, C. M. Cotten,

E. F. Donovan, R. A. Ehrenkranz, R. Guillet, R. D. Higgins, Aggressive vs. conservative phototherapy for infants with extremely low birth weight. *N. Eng. J. Med.* **359**, 1885–1896 (2008).
14. P. W. Chang, M. W. Kuzniewicz, C. E. McCulloch, T. B. Newman, A clinical prediction rule for rebound hyperbilirubinemia following inpatient phototherapy. *Pediatrics* **139**, e20162896 (2017).
15. T. Xiong, Y. Qu, S. Cambier, D. Mu, The side effects of phototherapy for neonatal jaundice: What do we know? What should we do? *Eur. J. Pediatr.* **170**, 1247–1255 (2011).
16. V. K. Bhutani, G. R. Gourley, S. Adler, B. Kreamer, C. Dalin, L. H. Johnson, Noninvasive measurement of total serum bilirubin in a multiracial predischarge newborn population to assess the risk of severe hyperbilirubinemia. *Pediatrics* **106**, e17 (2000).
17. W. D. Engle, G. L. Jackson, E. K. Stehel, D. M. Sendelbach, M. D. Manning, Evaluation of a transcutaneous jaundice meter following hospital discharge in term and near-term neonates. *J. Perinatol.* **25**, 486–490 (2005).
18. M. J. Maisels, W. D. Engle, S. Wainer, G. L. Jackson, S. McManus, F. Artinian, Transcutaneous bilirubin levels in an outpatient and office population. *J. Perinatol.* **31**, 621–624 (2011).
19. K. Yamana, I. Morioka, D. Kurokawa, S. Fukushima, K. Nishida, S. Ohyama, N. Nishimura, K. Nozu, M. Taniguchi-Ikeda, H. Nagase, K. Fujioka, S. Iwatani, H. Nakamura, K. Iijima, Evaluation of biliCare™ transcutaneous bilirubin device in Japanese newborns. *Pediatr. Int.* **59**, 1058–1063 (2017).
20. J. A. Taylor, A. E. Burgos, V. Flaherman, E. K. Chung, E. A. Simpson, N. K. Goyal, I. Von Kohorn, N. Dhepyasuwan; Better Outcomes through Research for Newborns Network, Discrepancies between transcutaneous and serum bilirubin measurements. *Pediatrics* **135**, 224–231 (2015).
21. J. A. Taylor, J. W. Stout, L. de Greef, M. Goel, S. Patel, E. K. Chung, A. Koduri, S. McMahon, J. Dickerson, E. A. Simpson, E. C. Larson, Use of a smartphone app to assess neonatal jaundice. *Pediatrics* **140**, e20170312 (2017).
22. S. B. Munkholm, T. Krøgholt, F. Ebbesen, P. B. Szecsi, S. R. Kristensen, The smartphone camera as a potential method for transcutaneous bilirubin measurement. *PLOS ONE* **13**, e0197938 (2018).
23. L. Y. Chen, B. C.-K. Tee, A. L. Chortos, G. Schwartz, V. Tse, D. J. Lipomi, H.-S. P. Wong, M. V. McConnell, Z. Bao, Continuous wireless pressure monitoring and mapping with ultra-small passive sensors for health monitoring and critical care. *Nat. Commun.* **5**, 5028 (2014).
24. M. Ramuz, B. C.-K. Tee, J. B.-H. Tok, Z. Bao, Transparent, optical, pressure-sensitive artificial skin for large-area stretchable electronics. *Adv. Mater.* **24**, 3223–3227 (2012).
25. J. Kim, P. Gutruf, A. M. Chiarelli, S. Y. Heo, K. Cho, Z. Xie, A. Banks, S. Han, K.-I. Jang, J. W. Lee, K.-T. Lee, X. Feng, Y. Huang, M. Fabiani, G. Gratton, U. Paik, J. A. Rogers, Miniaturized battery-free wireless systems for wearable pulse oximetry. *Adv. Funct. Mater.* **27**, 1604373 (2017).
26. C. Xu, Y. Yang, W. Gao, Skin-interfaced sensors in digital medicine: From materials to applications. *Matter* **2**, 1414–1445 (2020).
27. W. Gao, S. Emaminejad, H. Y. Y. Nyein, S. Challa, K. Chen, A. Peck, H. M. Fahad, H. Ota, H. Shiraki, D. Kiriya, D.-H. Lien, G. A. Brooks, R. W. Davis, A. Javey, Fully integrated wearable sensor arrays for multiplexed *in situ* perspiration analysis. *Nature* **529**, 509–514 (2016).
28. K. Dong, X. Peng, Z. L. Wang, Fiber/fabric-based piezoelectric and triboelectric nanogenerators for flexible/stretchable and wearable electronics and artificial intelligence. *Adv. Mater.* **32**, 1902549 (2020).
29. T. Yokota, P. Zalar, M. Kaltenbrunner, H. Jinno, N. Matsuhisa, H. Kitanosako, Y. Tachibana, W. Yukita, M. Koizumi, T. Someya, Ultraflexible organic photonic skin. *Sci. Adv.* **2**, e1501856 (2016).
30. H. U. Chung, B. H. Kim, J. Y. Lee, J. Lee, Z. Xie, E. M. Ibler, K. Lee, A. Banks, J. Y. Jeong, J. Kim, C. Ogle, D. Grande, Y. Yu, H. Jang, P. Assem, D. Ryu, J. W. Kwak, M. Namkoong, J. B. Park, Y. Lee, D. H. Kim, A. Ryu, J. Jeong, K. You, B. Ji, Z. Liu, Q. Huo, X. Feng, Y. Deng, Y. Xu, K.-I. Jang, J. Kim, Y. Zhang, R. Ghaffari, C. M. Rand, M. Schau, A. Hamvas, D. E. Weese-Mayer, Y. Huang, S. M. Lee, C. H. Lee, N. R. Shanbhag, A. S. Paller, S. Xu, J. A. Rogers, Binodal, wireless epidermal electronic systems with in-sensor analytics for neonatal intensive care. *Science* **363**, eaau0780 (2019).
31. H. U. Chung, A. Y. Rwei, A. Hourlier-Fargette, S. Xu, K. Lee, E. C. Dunne, Z. Xie, C. Liu, A. Carlini, D. H. Kim, D. Ryu, E. Kulikova, J. Cao, I. C. Odland, K. B. Fields, B. Hopkins, A. Banks, C. Ogle, D. Grande, J. B. Park, J. Kim, M. Irie, H. Jang, J. Lee, Y. Park, J. Kim, H. H. Jo, H. Hahm, R. Avila, Y. Xu, M. Namkoong, J. W. Kwak, E. Suen, M. A. Paulus, R. J. Kim, B. V. Parsons, K. A. Human, S. S. Kim, M. Patel, W. Reuther, H. S. Kim, S. H. Lee, J. D. Leedle, Y. Yun, S. Rigali, T. Son, I. Jung, H. Arafa, V. R. Soundararajan, A. Ollech, A. Shukla, A. Bradley, M. Schau, C. M. Rand, L. E. Marsillio, Z. L. Harris, Y. Huang, A. Hamvas, A. S. Paller, D. E. Weese-Mayer, J. Y. Lee, J. A. Rogers, Skin-interfaced biosensors for advanced wireless physiological monitoring in neonatal and pediatric intensive-care units. *Nat. Med.* **26**, 418–429 (2020).
32. H. Chen, M. Xue, Z. Mei, S. Bambang Oetomo, W. Chen, A review of wearable sensor systems for monitoring body movements of neonates. *Sensors* **16**, 2134 (2016).
33. A. Azhari, S. Yoshimoto, H. Ota, Y. Noda, T. Araki, T. Uemura, K. Morii, T. Sekitani, A patch type wearable wireless forehead pulse oximeter for polysomnography, *2017 IEEE Biomedical Circuits and Systems Conference (BioCAS)* (Turin, 2017), pp. 1–4.
34. R. G. Haahr, S. B. Duun, M. H. Toft, B. Belhage, J. Larsen, K. Birkelund, E. V. Thomsen, An electronic patch for wearable health monitoring by reflectance pulse oximetry. *IEEE Trans. Biomed. Circuits Syst.* **6**, 45–53 (2012).
35. G. Inamori, Y. Isoda, Z. Song, A. Uozumi, S. Ito, H. Ota, *2019 IEEE 32nd International Conference on Micro Electro Mechanical Systems (MEMS)* (Seoul, Korea (South), 2019), pp. 541–543.
36. C. M. Lochner, Y. Khan, A. Pierre, A. C. Arias, All-organic optoelectronic sensor for pulse oximetry. *Nat. Commun.* **5**, 5745 (2014).
37. J. M. Bland, D. G. Altman, Statistical methods for assessing agreement between two methods of clinical measurement. *Lancet* **327**, 307–310 (1986).
38. M. R. Grubb, J. Carpenter, J. A. Crowe, J. Teoh, N. Marlow, C. Ward, C. Mann, D. Sharkey, B. R. Hayes-Gill, Forehead reflectance photoplethysmography to monitor heart rate: Preliminary results from neonatal patients. *Physiol. Meas.* **35**, 881–893 (2014).
39. D. B. MacLeod, L. I. Cortinez, J. C. Keifer, D. Cameron, D. R. Wright, W. D. White, E. W. Moretti, L. R. Radulescu, J. Somma, The desaturation response time of finger pulse oximeters during mild hypothermia. *Anaesthesia* **60**, 65–71 (2005).
40. W. D. Engle, G. L. Jackson, N. G. Engle, Transcutaneous bilirubinometry. *Semin. Perinatol.* **38**, 438–451 (2014).
41. W. Engle, G. Jackson, D. Sendelbach, D. Manning, W. Frawley, Assessment of a transcutaneous device in the evaluation of neonatal hyperbilirubinemia in a primarily hispanic population. *Pediatrics* **110**, 61–67 (2002).
42. K. Jangaard, H. Curtis, R. Goldbloom, Estimation of bilirubin using biliChek™, a transcutaneous bilirubin measurement device: Effects of gestational age and use of phototherapy. *Paediatr. Child Health* **11**, 79–83 (2006).
43. S. Swarna, S. Pasupathy, B. Chinnasami, N. M. D, B. Ramraj, The smart phone study: Assessing the reliability and accuracy of neonatal jaundice measurement using smart phone application. *Int. J. Contemp. Pediatr.* **5**, 285 (2018).
44. M. Aydın, F. Hardalaç, B. Ural, S. Karap, Neonatal jaundice detection system. *J. Med. Syst.* **40**, 166 (2016).
45. A. Miyamoto, S. Lee, N. F. Cooray, S. Lee, M. Mori, N. Matsuhisa, H. Jin, L. Yoda, T. Yokota, A. Itoh, M. Sekino, H. Kawasaki, T. Ebihara, M. Amagai, T. Someya, Inflammation-free, gas-permeable, lightweight, stretchable on-skin electronics with nanomeshes. *Nat. Nanotech.* **12**, 907–913 (2017).
46. J. Villar, L. C. Ismail, C. G. Victora, E. O. Ohuma, E. Bertino, D. G. Altman, A. Lambert, A. T. Papageorghiou, M. Carvalho, Y. A. Jaffer, M. G. Gravett, M. Purwar, I. O. Frederick, A. J. Noble, R. Pang, F. C. Barros, C. Chumlea, Z. A. Bhutta, S. H. Kennedy; International Fetal and Newborn Growth Consortium for the 21st Century (INTERGROWTH-21st), International standards for newborn weight, length, and head circumference by gestational age and sex: The newborn cross-sectional study of the INTERGROWTH-21st project. *Lancet.* **384**, 857–868 (2014).
47. L. G. Heney, J. L. Greenstein, Diffuse radiation in the galaxy. *Astrophys J.* **93**, 70–83 (1941).
48. H. Funamizu, T. Maeda, S. Sasaki, I. Nishidate, Y. Aizu, Simulation of spectral reflectances in human skin tissue using ray tracing and GPU-based Monte Carlo method. *Opt Rev.* **21**, 359–363 (2014).
49. F. Elsamnah, A. Bilgaiyan, M. Affiq, C. H. Shim, H. Ishidai, R. Hattori, Reflectance-based organic pulse meter sensor for wireless monitoring of photoplethysmogram signal. *Biosensors* **9**, 87 (2019).
50. S. W. Back, Y. G. Lee, S. S. Lee, G. S. Son, Moisture-insensitive optical fingerprint scanner based on polarization resolved in-finger scattered light. *Opt. Express* **24**, 19195–19202 (2016).
51. M. D. van Erk, A. J. Dam-Vervloet, F. A. de Boer, M. F. Boomsma, H. van Straaten, N. Bosschaart, How skin anatomy influences transcutaneous bilirubin determinations: An in vitro evaluation. *Pediatr. Res.* **86**, 471–477 (2019).
52. Y.-J. Choi, K.-W. Lee, Y.-C. Gil, K.-S. Hu, H.-J. Kim, Ultrasonographic analyses of the forehead region for injectable treatments. *Ultrasound Med. Biol.* **45**, 2641–2648 (2019).
53. A. Bashkatov, E. Genina, V. Tuchin, Optical properties of skin, subcutaneous, and muscle tissues: A review. *J. Innov. Opt. Heal. Sci.* **04**, 9–38 (2011).
54. S. L. Jacques, Optical properties of biological tissues: A review. *Phys. Med. Biol.* **58**, 37–61 (2013).
55. J. A. D. Atencio, S. L. Jacques, S. V. y Montiel, Monte Carlo modeling of light propagation in neonatal skin, in *Applications of Monte Carlo Methods in Biology, Medicine and Other Fields of Science* (IntechOpen, London, 2011), pp. 297–314.
56. T. Maeda, N. Arakawa, M. Takahashi, Y. Aizu, Monte Carlo simulation of spectral reflectance using a multilayered skin tissue model. *Opt. Rev.* **17**, 223–229 (2010).

Acknowledgments

Funding: This work was supported by the Japanese Science and Technology Agency, PRESTO Grant (number: JPMJPR18J2), the Takeda Science Foundation, Life Science Research Grants, MIC/SCOPE (number: 181603007), AMED under grant number 20hm0102085h0001, the Ogasawara research grant, and the Japan Agency for Medical Research and Development. H.O. acknowledges support from a Grant-in-Aid for Young Scientists (A) and Grant-in-Aid for Challenging Exploratory Research provided by the Japanese Society for the Promotion of Science. **Author contributions:** H.O. conceived the

research. G.I. designed and performed the experiments and analyzed the data. U.K. performed software design. Y.I. and F.N. performed electrical and mechanical designs. A.U. and S.I. contributed to the approval from the ethics committee. A.U. and Y.O. helped clinical experiments. R.M. and M.S. took and edited the video. G.I., H.O., and S.I. wrote the manuscript. S.I. and H.O. supervised and oversaw the project. **Competing interests:** H.O., Y.I., G.I., A.U., and S.I. are inventors on pending patent applications related to this work filed by the Yokohama National University and the Yokohama City University (JP patent application no. 2018-239555, filed 21 December 2018; PCT patent application no. PCT/JP2019/049449, filed 17 December 2019). The authors declare that they have no other competing interests. **Data and materials availability:** All data needed to evaluate the conclusions in the paper are present in the paper and/or the Supplementary Materials. Additional data related to this paper may be requested from the authors.

Submitted 18 August 2020
Accepted 21 January 2021
Published 3 March 2021
10.1126/sciadv.abe3793

Citation: G. Inamori, U. Kamoto, F. Nakamura, Y. Isoda, A. Uozumi, R. Matsuda, M. Shimamura, Y. Okubo, S. Ito, H. Ota, Neonatal wearable device for colorimetry-based real-time detection of jaundice with simultaneous sensing of vitals. *Sci. Adv.* **7**, eabe3793 (2021).